AGU PUBLICATIONS

Water Resources Research

RESEARCH ARTICLE
10.1002/2016WR018696

Key Points:
- Wavelet decomposition identifies the frequency/period of the climate signal in which the variabilities with time are significant
- Application of block K-NN simulation technique on the significant wavelet signals of climate indices is skillful
- The conditional simulation of streamflow based on teleconnecting climate indices such as sea surface temperature is skillful

Supporting Information:
- Supporting Information S1

Correspondence to:
S. T. Erkyihun,
solomon.erkyihun@colorado.edu

Citation:
Erkyihun, S. T., B. Rajagopalan, E. Zagona, U. Lall, and K. Nowak (2016), Wavelet-based time series bootstrap model for multidecadal streamflow simulation using climate indicators, *Water Resour. Res.*, *52*, 4061–4077, doi:10.1002/2016WR018696.

Received 4 FEB 2016
Accepted 4 MAY 2016
Accepted article online 6 MAY 2016
Published online 26 MAY 2016

Wavelet-based time series bootstrap model for multidecadal streamflow simulation using climate indicators

Solomon Tassew Erkyihun[1,2], Balaji Rajagopalan[1,3], Edith Zagona[1,2], Upmanu Lall[4], and Kenneth Nowak[5]

[1]Civil, Environmental and Architectural Engineering, University of Colorado, Boulder, Colorado, USA, [2]Center for Advanced Decision Support for Water and Environmental Systems, University of Colorado, Boulder, Colorado, USA, [3]Cooperative Institute for Research in Environmental Sciences, University of Colorado, Boulder, Colorado, USA, [4]Earth and Environmental Engineering, Columbia University, New York, New York, USA, [5]Bureau of Reclamation, Lower Colorado Region, Boulder City, Nevada, USA

Abstract A model to generate stochastic streamflow projections conditioned on quasi-oscillatory climate indices such as Pacific Decadal Oscillation (PDO) and Atlantic Multi-decadal Oscillation (AMO) is presented. Recognizing that each climate index has underlying band-limited components that contribute most of the energy of the signals, we first pursue a wavelet decomposition of the signals to identify and reconstruct these features from annually resolved historical data and proxy based paleoreconstructions of each climate index covering the period from 1650 to 2012. A *K*-Nearest Neighbor block bootstrap approach is then developed to simulate the total signal of each of these climate index series while preserving its time-frequency structure and marginal distributions. Finally, given the simulated climate signal time series, a K-Nearest Neighbor bootstrap is used to simulate annual streamflow series conditional on the joint state space defined by the simulated climate index for each year. We demonstrate this method by applying it to simulation of streamflow at Lees Ferry gauge on the Colorado River using indices of two large scale climate forcings: Pacific Decadal Oscillation (PDO) and Atlantic Multi-decadal Oscillation (AMO), which are known to modulate the Colorado River Basin (CRB) hydrology at multidecadal time scales. Skill in stochastic simulation of multidecadal projections of flow using this approach is demonstrated.

1. Introduction

Understanding streamflow variability and the ability to generate realistic scenarios at multidecadal time scales is important for robust water resources planning and management in any river basin, especially in semiarid basins such as the CRB. It is increasingly evident that large-scale climate forcings such as El Nino Southern Oscillation (ENSO), Pacific Decadal Oscillation (PDO), and Atlantic Multi-decadal Oscillation (AMO) modulate the hydroclimatology of the western United States at multidecadal time scales [*Tootle* et al., 2005, *Timilsena et al*., 2009; *Enfield et al*., 2001; *McCabe and Dettinger*, 1999, *McCabe et al*., 2007; *Hidalgo*, 2004; *Nowak et al*., 2012]. The influence of ENSO on the variability of precipitation and flows in western United States has been well documented [*Redmond and Koch*. 1991; *Timilsena et al*., 2009; *Dracup and Kahya*, 1994; *Thomson et al*., 2003]. The subtropical jet stream that funnels storms to this region during winter, which is the major source of moisture, is intensified over the southwestern U.S. during El Nino events, bringing more rain and snow to this region while drying the northwestern U.S. and vice-versa during La Nina events. This causes significant interannual variability in precipitation and stream flow. However, its direct impact on the Colorado Basin is weaker [e.g., *Regonda et al*., 2006; *Grantz et al*., 2005]. The PDO is a decadal phenomenon [*McCabe et al*., 2004, 2007, 2008] that has been shown to influence western United States hydroclimatology along with ENSO over interannual and multidecadal time scales [*Gershunov and Barnett*, 1998, *Rajagopalan et al*., 2000]. The positive phase of PDO with increased sea surface temperatures over the northern Pacific is generally associated with increased flow in the central and western United States, and the negative phase with decreased flow [*Tootle et al*., 2005; *Hidalgo*, 2004; *Timilsena et al*., 2009]. Recent research indicates strong connections between AMO and hydroclimatolgy over the United States. The warm phase of Atlantic Multidecadal Oscillation (AMO) is known to be associated with decreased flow conditions over most of the United States [*Enfield et al*., 2001; *Tootle et al*., 2005; *Timilsena et al*., 2009]. AMO is also known to modulate

the decadal to multidecadal variability of flow in the upper Colorado River Basin [*McCabe and Dettinger*, 1999, *McCabe et al*., 2007; *Hidalgo*, 2004; *Nowak et al*., 2012]. While ENSO, AMO, and PDO drive western United States hydroclimatology as evidenced by many researchers, AMO and PDO are the dominant drivers of flows in the Upper Colorado River Basin at interannual and decadal time scales as recently demonstrated by *Nowak et al*. [2012] and *Bracken et al*. [2014]. Lower Colorado Basin flows are also modulated by these climate forcings [*Thomas*, 2007].

There is a rich history of traditional time series simulation techniques [*Salas et al*., 1980; *Wei*, 2006] that fit linear models to the flow series. These models have done well when the hydrologic data did not exhibit long memory or nonlinear dependence, or quasi-oscillatory dynamics, or was not easily transformed to a Gaussian marginal distribution using the commonly used transforms. Nonparametric approaches were proposed to improve upon these methods to better reproduce nonlinear and non-Gaussian features in a Markovian context [*Lall*, 1995; *Lall and Sharma*, 1996; *Sharma et al*., 1997]. A second approach that was introduced at about the same time was the use of a moving block bootstrap [*Vogel and Shallcross*, 1996] to address non-Markovian dependence. Subject to the choice of a block length, this method allows time series simulation that incorporates some long memory characteristics. However, it does not lend itself to conditioning on climate indices or other predictors of the time series of interest. Subsequently, wavelet-based autoregressive moving average methods were introduced to address the modeling of quasi-oscillatory dynamics *Kwon et al*. [2007]. Their approach was to decompose the time series into a small set of quasi-periodic components [*Torrence and Compo*, 1998] and a residual time series. A traditional autoregressive moving average model is then fit to each of the components, including the residual process. The components are simulated and summed to obtain simulations of the original series. This method performed very well in capturing the global spectral properties, but not the nonstationarity of the spectrum. *Nowak et al*. [2011] enhanced this approach by scaling the components with their scale-averaged wavelet power, a time varying variance of the components, before fitting the autoregressive models, and then rescaling the simulated components with the same. This approach captured the nonstationarity in the spectrum very well. Recently, *Bracken et al*. [2014] showed that regime-like behavior of the Colorado River flows are forced by AMO and PDO, and used a nonhomogeneous hidden Markov model to simulate the flow properties using these two climate forcings.

Given this background, we present a novel algorithm, WKNN that stands for Wavelet-K-Nearest Neighbor, that integrates the recently developed wavelet and bootstrap features mentioned above. As in *Kwon et al*. [2007], a wavelet projection is used to decompose each climate index into a small set of components, each of which explains a statistically significant fraction of the variance of the time series and is limited to a specific frequency band. Each component time series is then modeled using a K-Nearest Neighbor (*K*-NN) block bootstrap method that is introduced. The goal of the method is to conditionally draw a block from the component time series given a current state vector. The *K*-NNs of the current state vector are used to provide samples of the conditioning distribution, from this a block of time series values that succeeds one of these *K*-NNs is then drawn at random, thus providing a conditional block bootstrap. A repeated application of this procedure allows one to develop a full time series with the appropriate time-frequency variability for the component time series. The component time series are then summed to provide a simulation of the climate index of interest. Once the climate index time series are available, annual flows for each year are simulated using the *K*-NN bootstrap approach [*Lall and Sharma*, 1996], conditional on the state space defined by that year's simulated climate indices. Following this procedure, we are able to maintain the time frequency structure of the climate indices and of the conditional distribution of annual flows given the climate indices.

The *K*-NN bootstrap approach was proposed by *Lall and Sharma* [1996] and applied to monthly streamflow simulation (i.e., lag-1 model). This method has been applied to multivariate stochastic weather generation [*Rajagopalan and Lall*, 1999; *Yates et al*., 2003; *Caraway et al*., 2014], paleostreamflow reconstruction [*Gangopadhyay et al*., 2009], water quality modeling [*Towler et al*., 2009], and others. The idea of resampling blocks of *B* capitalizes on the fact that there is significant dependence in the climate signals of at least lag *B* that needs to be captured. Typical literature on block bootstrapping as described by *Efron and Tibishirani* [1993] is unconditional or without the feature vector and the neighbor selected as described above. Random block size using a geometric distribution, more suitable for weakly dependent data, was proposed by *Politis and Romano* [1994] and used recently to model dependency in paleo streamflow by *Razavi et al*.

[2015]. For WKNN, we incorporated the feature vector to better capture nonstationarity. The modification with block resampling combined with wavelet components is unique and the novel aspect of this research.

The paper is organized as follows. The data used in this research is presented first followed by the methodology and its components. Model validation is described and then the results. The summary of the results and discussion conclude the paper.

2. Data

The historical and paleodata of annual Colorado River streamflow and annual climate indicators are described below.

2.1. Colorado River Flow at Lees Ferry, AZ

The Lees Ferry flow gauge, through which 90% of the naturalized flow in the basin passes, divides the Colorado River Basin into the upper and lower operational basins. Naturalized water year flows (sum of flows during October–September) at this gauge for the period 1906–2012 are used in this study. Monthly naturalized flow is computed by removing anthropogenic effects such as regulation and diversions. It is updated regularly by the United States Bureau of Reclamation [*Prairie and Callejo*, 2005] (http://www.usbr.gov/lc/region/g4000/NaturalFlow/current.html). The data have been used for planning studies in the basin [*Reclamation*, 2012] and in other research [*Regonda et al*., 2011; *Nowak et al*., 2011; *Miller et al*., 2012]. In addition, tree ring reconstructed flows for the pre-1906 period covering 1490–1905 from *Woodhouse et al*. [2006] are also used in this study. The reconstructed data are available here: http://treeflow.info/upco/coloradoleeswoodhouse.txt.

2.2. Climate Indices, AMO and PDO

The AMO index [*Enfield et al*., 2001] is computed as a monthly area-weighted average of North Atlantic (0–70°N) sea surface temperatures (SST), which is subsequently detrended, based on 5° × 5° resolution Kaplan SST [*Kaplan et al*., 1998]. Values were obtained from the NOAA Physical Sciences Division website http://www.esrl.noaa.gov/psd/data/timeseries/AMO/ for the period 1856 to present. The paleoreconstruction of annual AMO for the period (1650–1990) is based on reconstructions of annual sea surface temperature anomalies (SSTA) for the North Atlantic Ocean (0–70°N) from tree rings [*Gray et al*., 2004] and was obtained from the NOAA website ftp://ftp.ncdc.noaa.gov/pub/data/paleo/treering/reconstructions/amo-gray2004.txt.

Monthly PDO anomalies from 1900 to present are available from the University of Washington (http://jisao.washington.edu/pdo/PDO.latest). The annual data were taken as the average of the monthly (averaged over October–September, to be consistent with the flow) values in this analysis. The PDO is calculated as the first principal component of the Northern Pacific SST [*Zhang et al*., 1997; *Mantua et al*., 1997]. Annual PDO values for the period 993–1996, based on tree rings from *Pinus flexilis* in California and Alberta, Canada, were generated by *MacDonald and Case* [2005] and are available from the NOAA website ftp://ftp.ncdc.noaa.gov/pub/data/paleo/treering/reconstructions/pdo-macdonald2005.txt.

In summary, we use historical and paleoreconstructed records that cover a common period from 1650 to 2012 for the Colorado River flow at Lees Ferry, the AMO and the PDO. We refer the period 1650–2012 as long historical and the period 1906–2012 as historical.

3. Proposed Methodology

The methodology we propose has three broad steps: (i) Decompose the large-scale climate indices to obtain dominant signals in specific frequency bands that explain a statistically significant fraction of the signal's variance [*Torrence and Compo*, 1998; *Kwon et al*., 2007]. (ii) Simulate these dominant signals independently using a new block *K*-NN bootstrap approach. We refer to these two steps as WKNN; and (iii) Simulate the streamflow using *K*-NN bootstrap conditioned on the simulated climate forcings [*Lall and Sharma*, 1996] from the previous step. These steps are described below.

3.1. WKNN: Wavelet Decomposition

The first step is to decompose the climate indices using wavelets into orthogonal quasi-periodic components. For a detailed exposé on wavelet analysis for geophysical applications, we refer to *Kumar and Foufoula-Georgiou* [1994, 1997]. Here we follow the implementation procedures described in [*Torrence and Compo*, 1998; *Kwon et al*., 2007; *Nowak et al*., 2011]. A brief description is provided here.

The continuous wavelet transform of a discrete time series for a period a and time n, is given by:

$$W_n(a) = \sum_{j=0}^{N-1} \hat{x}_j \hat{\psi}^*(a\omega_j) e^{i\omega_j n\delta_t} \tag{1}$$

where $\hat{x}_j$ is the discrete Fourier transform of the original time series; $\hat{\psi}^*(a\omega_j)$ is the Fourier transform of the wavelet function, ψ; N is the number of data points in the original data; δ_t is the time factor or time step (for annual data it is equal to 1); and ω is the angular frequency.

The Morlet is chosen to be the preferred wavelet function for its boundary properties [*Torrence and Compo*, 1998] and its simplicity for time series applications. It is given by:

$$\psi_0(\eta) = \pi^{-1/4} e^{i\omega_0\eta} e^{-\eta^2/2} \tag{2}$$

where ω_0 and η are the nondimensional frequency and time parameters, respectively [*Torrence and Compo*, 1998]. Since we use the Morlet wavelet, $\omega_0 = 5$ is chosen [*Kumar and Foufoula-Georgiou*, 1997]. We compared wavelet spectra and time series simulations from two other wavelets—DOG and Paul—and found that the performance of the simulations were virtually identical. The wavelet choice does not seem to influence the time series simulation.

The wavelet spectrum represents the power at a period a and time t. In the wavelet literature, the period a is referred to as the scale. We refer to this as the period in the context of the quasi-oscillatory modes of the time series used in this research. Averaging this across time provides the global wavelet spectrum. Tests of the statistical significance of the power at a given period are typically based on a null hypothesis of a white or red noise process [*Torrence and Compo*, 1998]. Here we used white noise for the null hypothesis. The global and nonstationary spectra of AMO and PDO are shown in Figures 1 and 2, respectively. Figures 1a and 1b show the wavelet spectra of AMO for the observational and paleo periods, respectively. The white noise based confidence levels are shown for the global spectrum. Significant power can be seen in the 32–128 year period and longer for the paleorecord. For the PDO (Figure 2), the multidecadal band of 8–32 year period is dominant in recent decades in the historical period and sustained throughout the long-historical period. The variation of PDO over a broad range of timescales is consistent with *Steinman et al*., [2015]. For the longer periods, the data are limited and thus, as indicated by the cone of influence, claims of significance of the power are not supported.

A component signal representing a frequency band where statistically significant power is identified is reconstructed as:

$$x_n' = \frac{\delta_j \delta_t^{1/2}}{C_\delta \psi_0(0)} \sum_{j=j_1}^{j_2} \frac{R\{W_n(a_j)\}}{a_j^{1/2}} \tag{3}$$

where C_δ and δ_j are reconstruction and scale factors, respectively. $\psi_0(0) = \pi^{-1/4}$ is the factor that removes the energy scaling for Morlet wavelet function; R denotes the real part of the wave; and a_j is the scale. The j_1 and j_2 are the lower and upper limits of the frequency range over which the average is computed. For example, in the case of PDO this would correspond to the 8 and 32 year periods, for j_1 and j_2, respectively. Similarly all other component signals are reconstructed representing the various significant frequency bands. Together they represent the total signal component.

3.2. WKNN: Simulating the Climate Signal Using Block Bootstrap

The steps are described below for simulating a sequence of a component signal of a climate index:

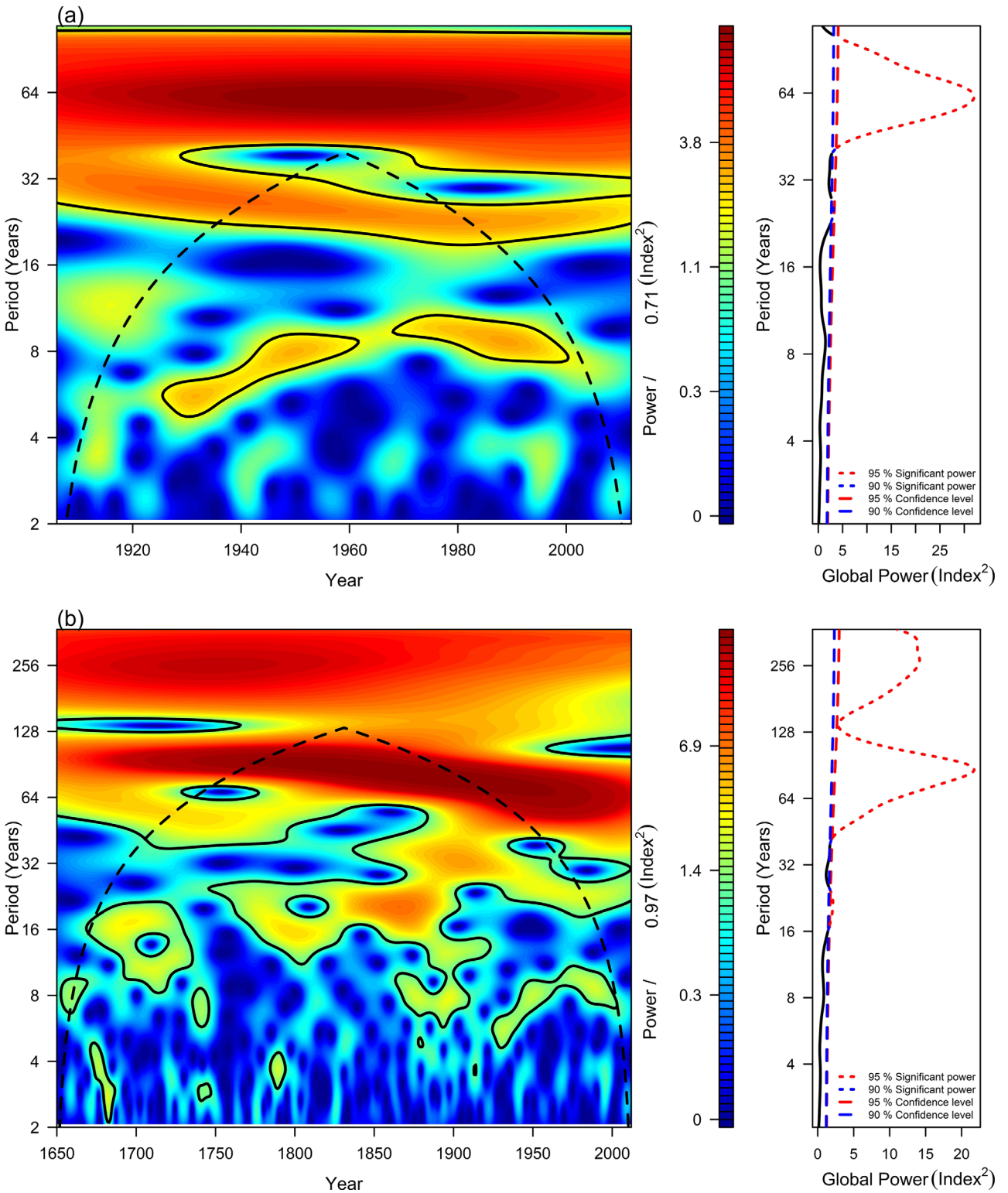

Figure 1. (a) Wavelet spectra of historical (1906–2012) AMO and (b) Wavelet spectra of the long historical (1650–2012) AMO. (left) Local power spectrum; the blue color demonstrates the lower power spectra and the red color the higher, and the dotted line is the cone of influence. The right-hand side plot is the global power spectrum with 90% and 95% confidence level from white noise. Index refers to the standardized AMO.

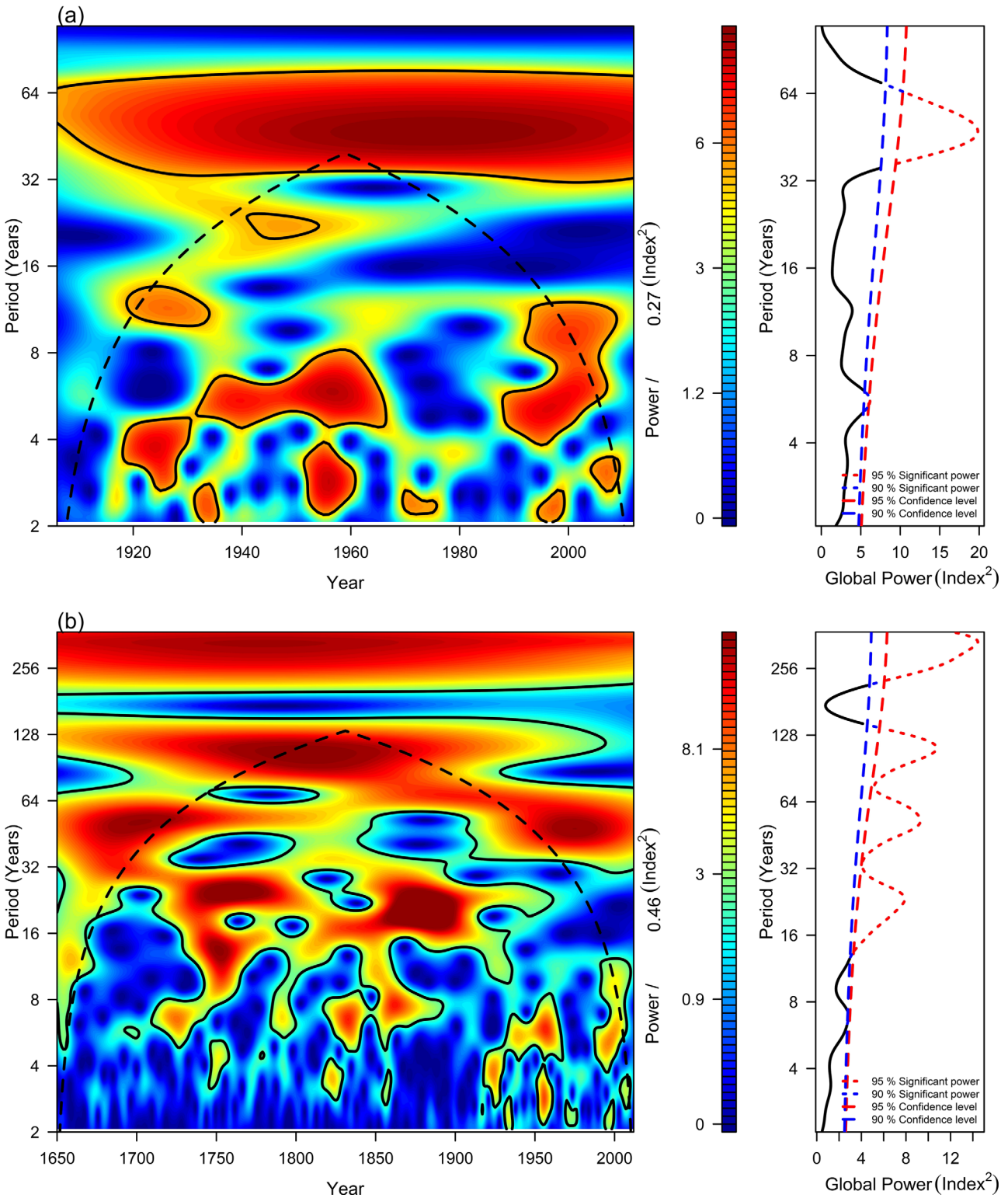

Figure 2. (a) Wavelet spectra of historical (1906–2012) PDO and (b) Wavelet spectra of the long historical (1650–2012) PDO. (left) Local power spectrum; the blue color demonstrates the lower power spectra and the red color the higher, and the dotted line is the cone of influence. The right-hand side plot is the global power spectrum with 90% and 95% confidence level from white noise. Index refers to the standardized PDO.

1. For each reconstructed component signal, the characteristic period, $\bar{P}$, is identified, as: $\bar{P}=\frac{j_1+j_2}{2}$ where j_1 *and* j_2 are upper and lower periods of the reconstructed signal. Then a block size, B, is computed which is quarter of $\bar{P}$.
2. For a given time t, a 'feature vector' of length B is created as $[x_t, x_{t-1}, \ldots x_{t-B+1}]$, where x_t is the climate signal at time t and K-NN of this feature vector based on Euclidean distance are identified in the full record of the reconstructed component signal time series. Since AMO and PDO are block bootstrapped separately, at a given time their joint vector is unlikely to be identical to any historical time. Hence the current vector is considered in the simulation.
3. One of the K-Nearest Neighbors is randomly selected using a probability metric described in [*Lall and Sharma*, 1996] as:

$$W_i=\frac{\frac{1}{i}}{\sum\frac{1}{i}};\ \ i\ =1,2,.,K \tag{4}$$

   Lall and Sharma [1996] proposed a heuristic choice for K as, $K=\sqrt{N}$ where N is the number of data points.

4. Suppose the neighbor j is selected which corresponds to a calendar time T. A sequence of time series values for a block of length B that follows, i.e., $x_{T+1},\ x_{T+2},\ \ldots,\ x_{T+B}$ then constitutes the simulated values for the succeeding B time steps $T+1$, $T+2$,. . ., $T+B$.
5. The simulated block becomes the new feature vector and steps (ii) through (iv) are repeated to simulate the signal for time steps $t+B+1$, $t+B+2, \ldots, t+2B$

The above steps are repeated to generate a sequence of any desired length B time steps at a time.

The above steps are applied to simulate sequences of all the reconstructed component signals. These simulated sequences of component signals are added to obtain the sequence of total signal. This is done for each climate index separately, i.e., AMO and PDO, thus resulting in a sequence of simulated climate signal vector for each time, $Y_t = [AMO_t, PDO_t]$.

3.3. Streamflow Simulation: Conditioned on Climate Signals

For each year (or time t), conditioned on the simulated climate signal vector, the streamflow needs to be simulated. This can be viewed as simulation from the conditional probability density function: $f(flow_t|Y_t)$ where the vector $Y_t = [AMO_t, PDO_t]$ is the vector of signals of climate indices at time t, as described in the previous section. The K-NN of Y_t are found from the historical reconstructed climate signal time series and one of the neighbors (i.e., a historical year) is selected using the K-NN probability metric in equation (4). The streamflow of the selected year becomes the simulated flow for time t. This is repeated for each year to generate an ensemble of streamflow sequences.

4. Model Validation

We applied the methods of the previous section to simulate Lees Ferry streamflow using the two climate indices, AMO and PDO. We tested the model in two modes: (i) ability to simulate the primary statistics of the series and, (ii) the ability to simulate multi-decadal projections.

Since the climate indices are simulated based on low-frequency components, the block bootstrap has relatively fewer blocks to select from when simulating for the historical period (1906–2012) using historical data. To demonstrate that this is not an issue, we simulated one of the climate indices, PDO, using WKNN with the longer historical period 1650–2012 and computed a suite of distributional and spectral statistics for comparison.

Then we applied it to the historical naturalized streamflow, 1906–2012 (107 years), wherein WKNN was applied to generate 500 ensembles of the two climate signals, each of length 107 years. For each simulated climate signal vector, using K-NN resampling, streamflow values are generated. This validation approach is typical of any stochastic time series model in that the models are fitted to the data and simulations are made from them. A suite of distributional statistics of the simulated flow sequences is computed from the simulations—mean, variance, lag-1 autocorrelation, probability density functions (PDFs), and wavelet spectra—and compared with those of the historical record. The wavelet spectrum is computed for the median flow of the simulations (i.e., median of ensemble of simulations at each time step) for comparison with the

wavelet spectrum of the historical data. This demonstrates the ability of the method to capture the statistics and nonstationarity in the variability of the time series.

5. Results

We first applied the WKNN approach directly to the Lees Ferry flows and generated simulations for the historical period. In this, the component signals of the flows were generated using block bootstrap and subsequently the noise (or residual) component was simulated using a lag-1 *K*-NN bootstrap [*Lall and Sharma*, 1996] and added to obtain the complete flow variance. The simulations could not capture the nonstationarity in the spectrum and did somewhat poorly on other statistics (figures not shown). This is mainly due to the fact that the variance of the flow in the signal components was just ∼45% and a substantial proportion (∼65%) in the noise. The noise component, simulated with no temporal structure, unlike the signal components with block bootstrap, destroys the nonstationary features. However, simulating streamflow as a consequence of simulations of teleconnecting large-scale climate forcings alleviates this problem and appears to perform skillfully as described below.

5.1. Climate Index Simulation

The component signals of AMO are based on the period ranges of 23–27 years and 40–90 years (Figure 1); while those of PDO are based on 20–27 years and 40–90 years (Figure 2). The higher period ranges are outside the cone of influence, more so during the historical period, but they are within for the most part during the long historical period. Furthermore, the relationship between these indices and the Lees Ferry flow in these general period bands has been shown by others [*Nowak et al*., 2011; *Switanek and Troch*, 2011]. The spectral power of the climate indices shows temporal variability (Figures 1 and 2) as mentioned above, indicative of nonstationarity which also induces quasi-periodicity. The nonstationarity in the flows will be described later. Our objective here is to simulate the flow conditioned on these signals and, to the extent they are significant, we exploit their quasi-periodic behavior and links to flow.

As mentioned, in order to test the performance of the WKNN model in simulating the climate indices, we first demonstrated on the simulations of the climate index, PDO, for the long historical period (1650–2012 using both the paleo and observed data). Simulating the longer period allows for a rich variety of blocks to be resampled. The component signals are simulated using the block bootstrap approach described in the methodology section and the residuals are simulated using a lag-1 *K*-NN bootstrap [*Lall and Sharma*, 1996], for consistency. However, a standard lag-1 auto regressive model (AR1) was also tested and the results were quite similar. Thus simulated PDO sequences were used to compute a suite of statistics and compared with the historical data. We show results from simulations of PDO; the performance of simulations from AMO is similar. Figure 3 shows the boxplots of basic distributional statistics—mean, variance, skewness, and lag-1 autocorrelation of simulated PDO with the long historical values shown as red dots. It can be seen that the simulations capture the observed statistics within the interquartile range, except for variance and lag-1 autocorrelation which are under simulated. However, the actual difference between the historical value and the median of the simulations is quite small ∼0.2 for variance and ∼0.09 for lag-1 autocorrelation. Figure 4 shows the simulated and historical PDF, which also is seen to be captured quite well, with the simulated PDF being more symmetric. The wavelet spectrum of the historical data and the median spectrum from the simulations are shown in Figures 5a and 5b, the global spectra are on the side of these plots. It can be seen that the local and global spectra are very well simulated. All four spectral peaks in the historical period (Figure 5a) are captured well in the simulations (Figure 5b). Furthermore, the nonstationarity in the spectrum—the 32–64 year band being active during 1650–1750 and then during 1950–present (Figure 5a)—is well captured in the simulations (Figure 5b). Similarly the 16–32 year band which is active during 1750–1900 and weaker in recent decades is also well captured by the simulations. The variance of the PDO index present in the signal components is ∼51% and the noise component has ∼49% of the total PDO variance. A higher signal variance enables the WKNN to capture the distributional and spectral features better than the application of WKNN directly on the flows as mentioned above. These results demonstrate the capability of WKNN in simulating distribution and nonstationary features of the signal of climate indices—which are important to generate sustained wet/dry sequences of the flows.

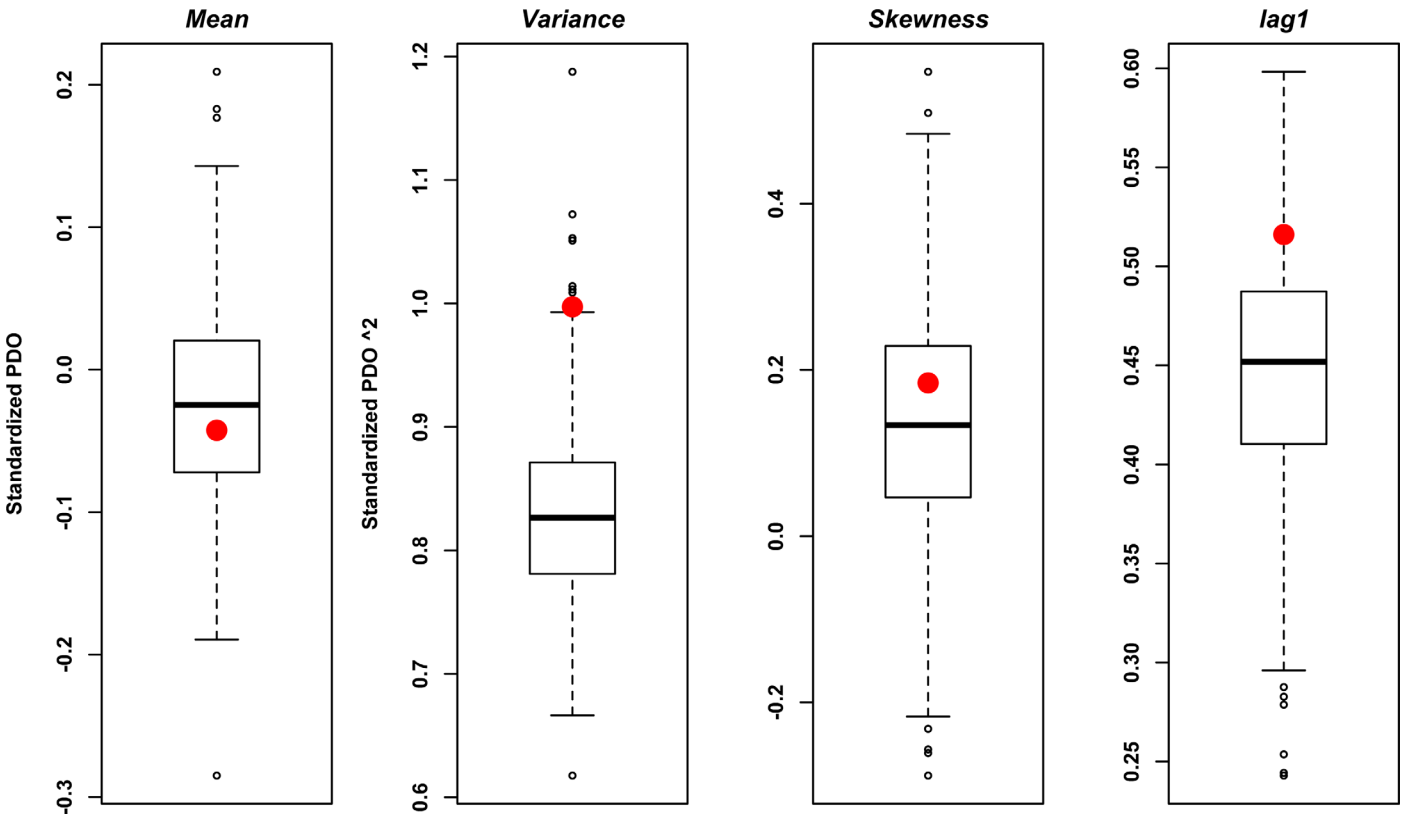

Figure 3. Boxplots of basic distributional statistics from the long historical (1650–2012) PDO simulations, red dot is the corresponding value of the long historical period.

5.2. Lees Ferry Streamflow Conditional Simulations

We used the WKNN to simulate PDO and AMO for the historical period (1906–2012) and conditionally simulate the streamflow. Figure 6 shows the boxplots of distributional statistics from flow simulations along with the historical values. It can be seen that the simulations reproduce very well the basic statistics—mean, variance skew, and lag-1 autocorrelation. We note that the lag-1 correlation in the streamflow is entirely simulated from the climate indices—considering this, the simulations are quite good. The boxplots of the PDF (Figure 7) from the simulations also capture the historical PDF very well, indicating that the shape of the distribution and, consequently, the cumulative distribution function is also reproduced.

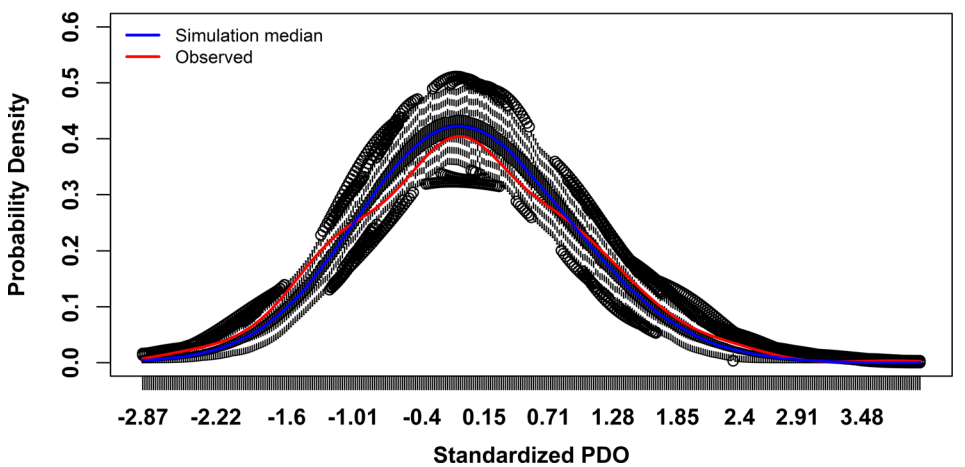

Figure 4. Probability Density Functions of the long historical PDO simulation shown as boxplots, the blue line is the median PDF and the red is from the historical data.

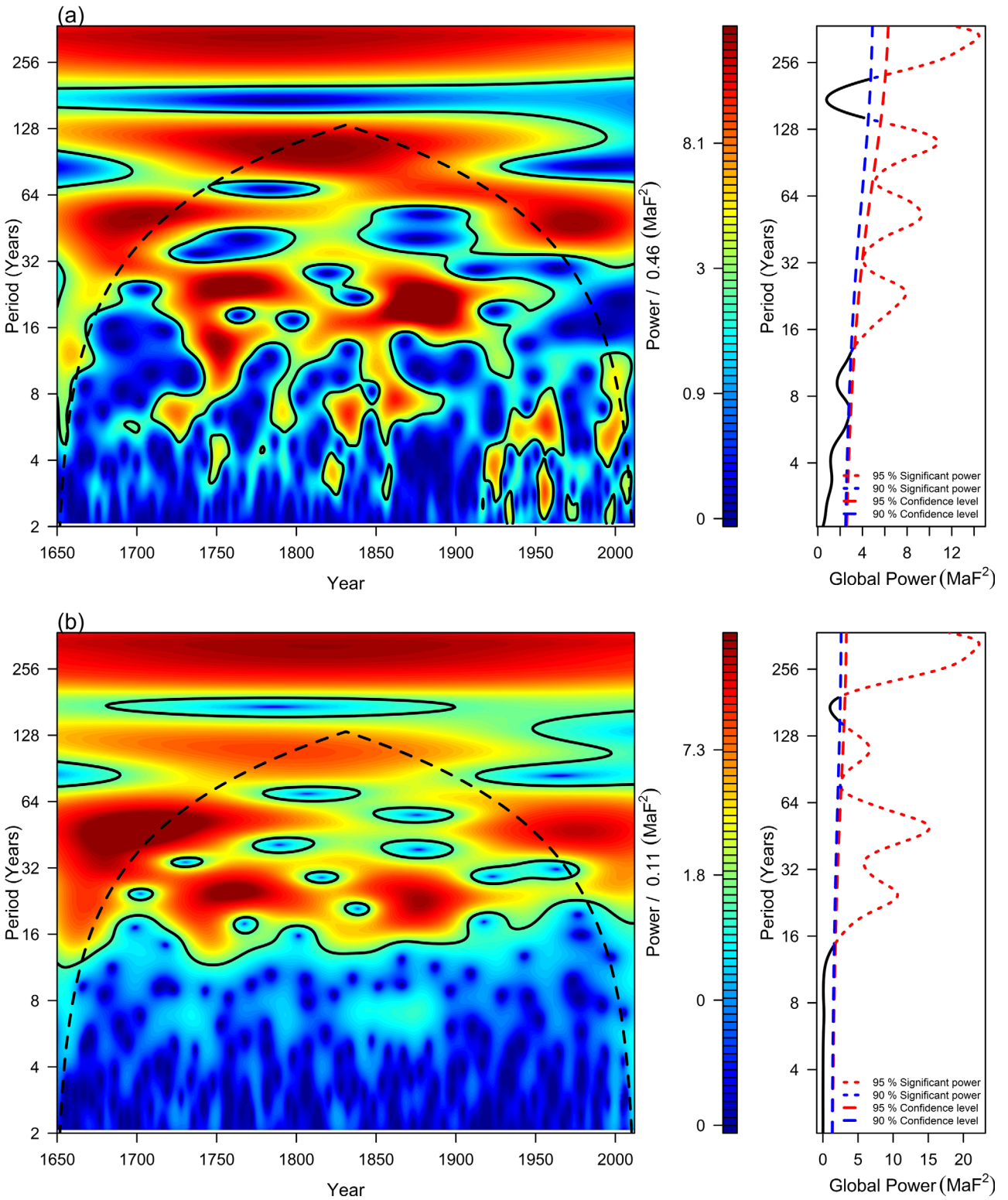

Figure 5. (a) Power spectrum of long historical (1650–2012) PDO—local spectrum on the left and global on the right, (b) Same as Figure 5a but median spectrum of PDO from the WKNN simulations.

Crossing or threshold exceedance and nonexceedance statistics are nonlinear and typically not expected to be captured in the simulations as they are not explicit in the model. These are complementary statistics in characterizing the flow sequences useful for planning. We calculated the excess and deficit statistics based

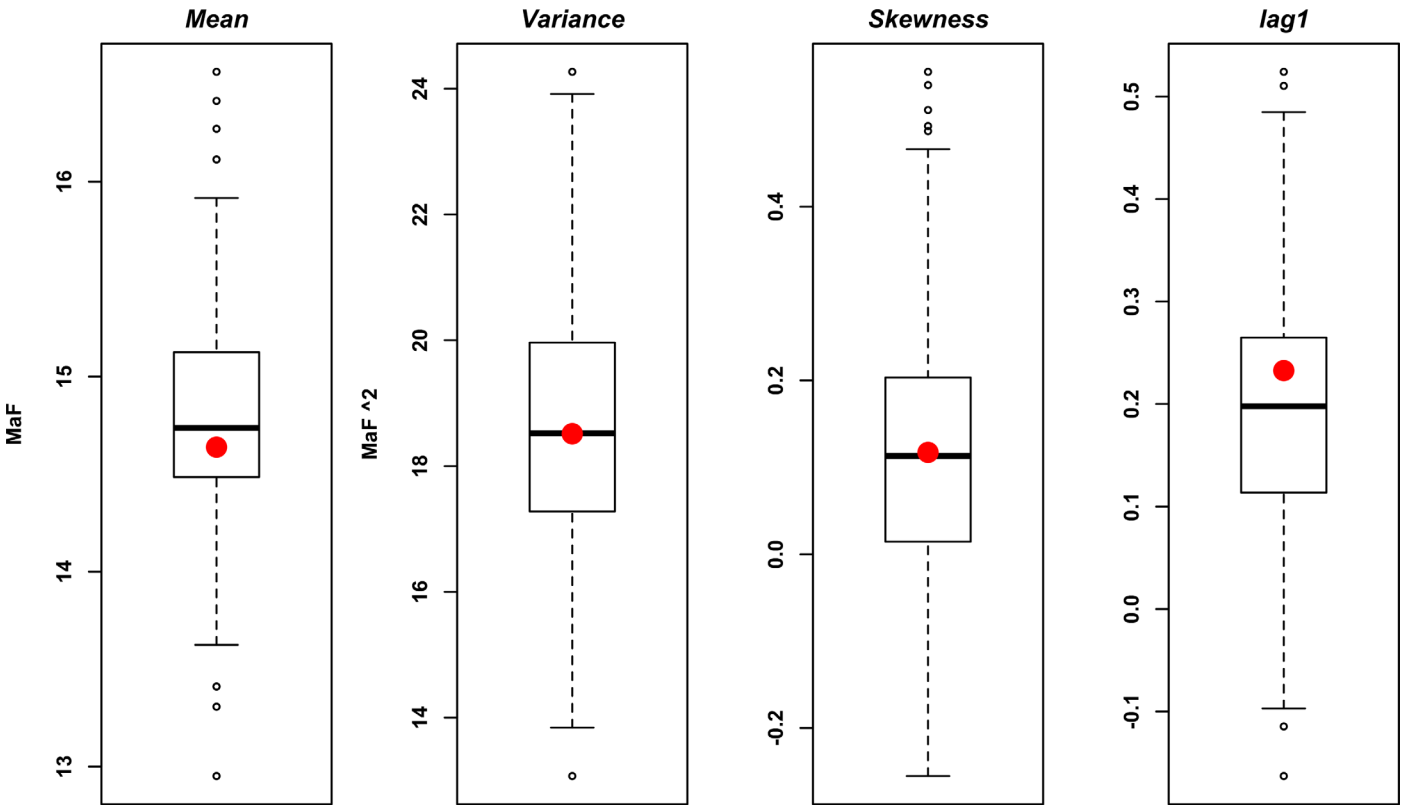

Figure 6. Boxplots of basic distributional statistics from the Lees Ferry flow simulations, red dot is the corresponding value of the historical period (1906–2012).

on the median annual flow of the historical period (1906–2012), 14.52 million acre feet (MAF). Excess is defined as the magnitude of flow in excess of the median and deficit as the magnitude less than the median. We computed the total, maximum, and minimum magnitudes of the excess and deficit sequences to assess the ability of the simulation in capturing these spell quantities. The boxplots of these statistics from the simulations are shown in Figure 8 along with the corresponding values from the historical sequence as red dots. It can be seen that the deficit and excess statistics are asymmetric with lower values for the deficit and higher for the excess indicative of how well they are reproduced by the simulations.

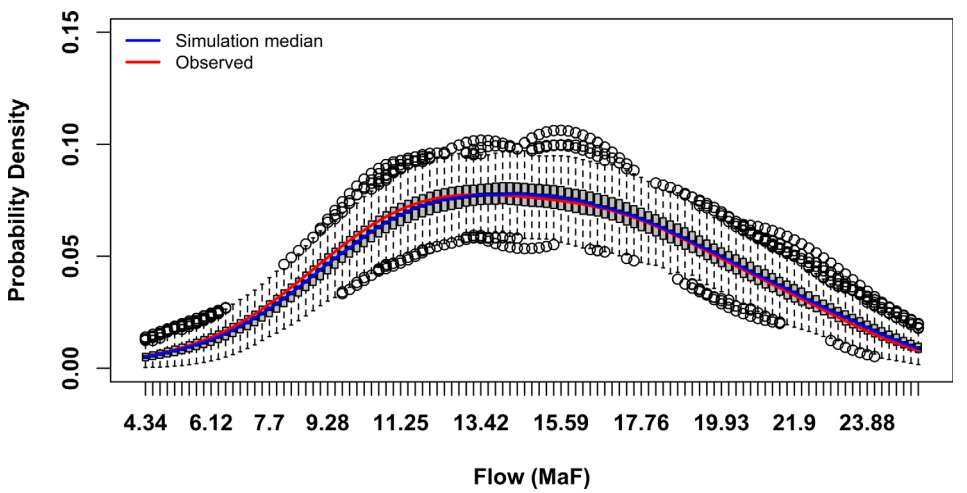

Figure 7. Probability Density Functions of simulated Lees Ferry flow shown as boxplots, the blue line is the median PDF, and the red is from the historical period.

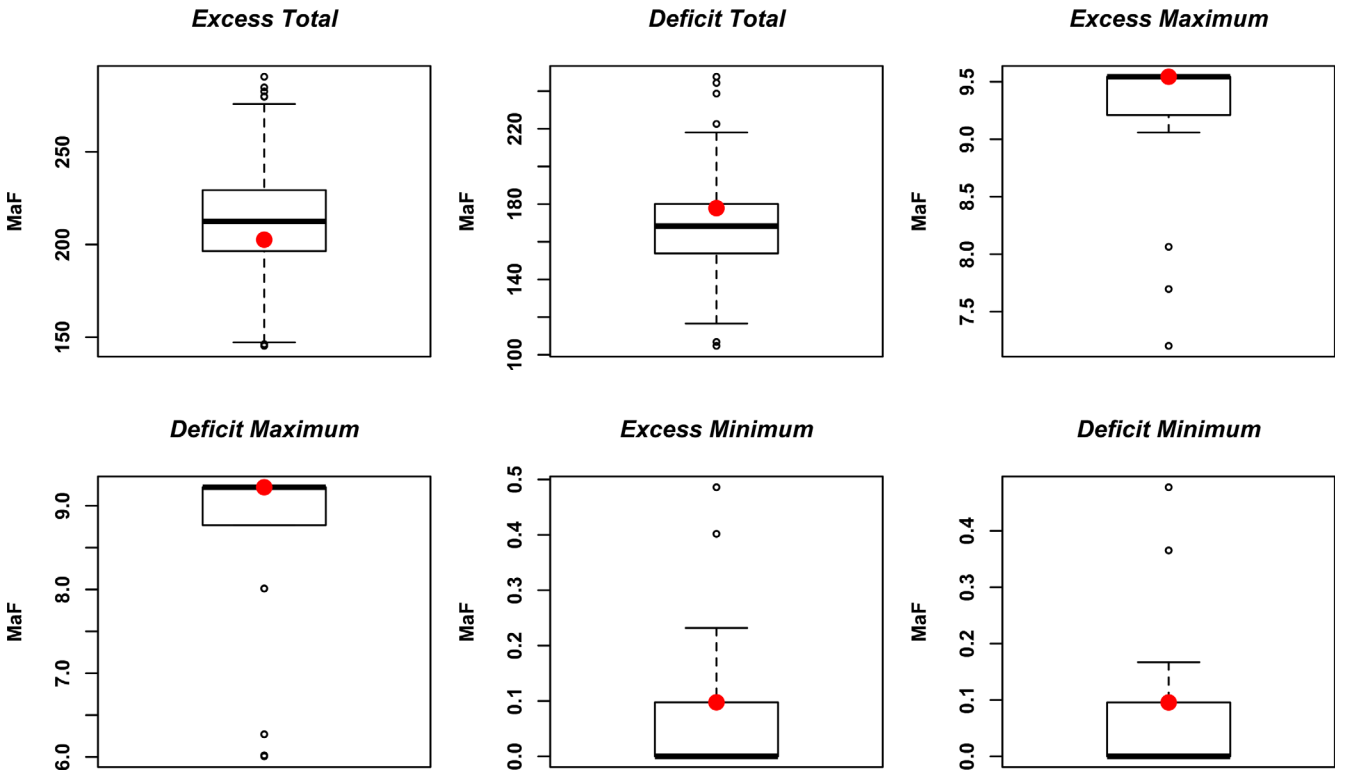

Figure 8. Boxplots of deficit and excess statistics from the simulations along with the corresponding values based on historical period shown as red dots.

To further assess the performance of the simulations in capturing wet and dry sequences which are crucial for water resources management, we computed storage statistics using the sequent peak algorithm [*Loucks and Van Beek*, 2005]. In this, for a given flow sequence and a selected demand (or yield) to be met, the required reservoir storage is computed. Thus, a storage-yield curve is obtained for several demand scenarios. The effect of critical droughts is captured in this approach. Figure 9 shows the boxplots of storage for different demand levels from the simulations along with that from the historical flow sequence. It can be seen that the storage from the historical flow sequence (red dots) is very well captured within the boxes, indicating that the simulations are able to reproduce the stretches of wet and dry sequences that are important in the storage calculations and in facilitating robust long-term planning.

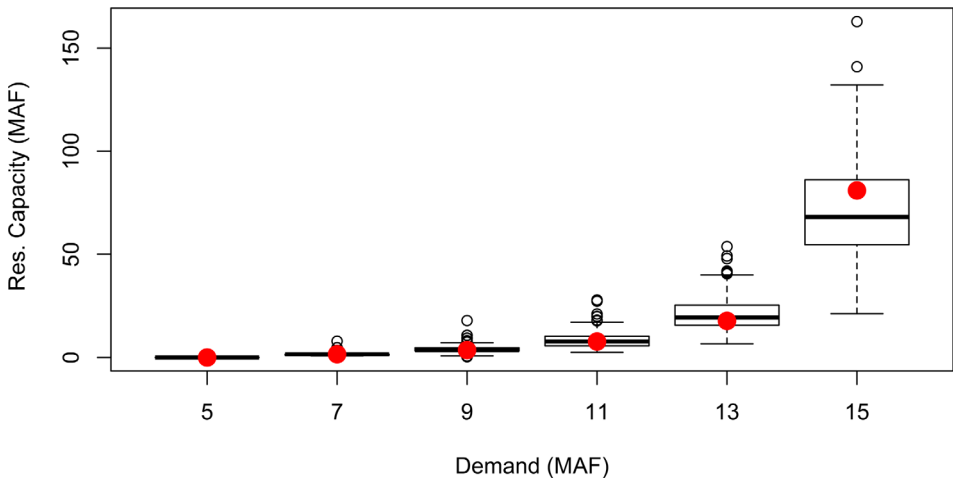

Figure 9. Boxplots of required storage for several demand values calculated by the sequent peak algorithm, based on the flow simulations. Storages from the historical data are shown as red dots.

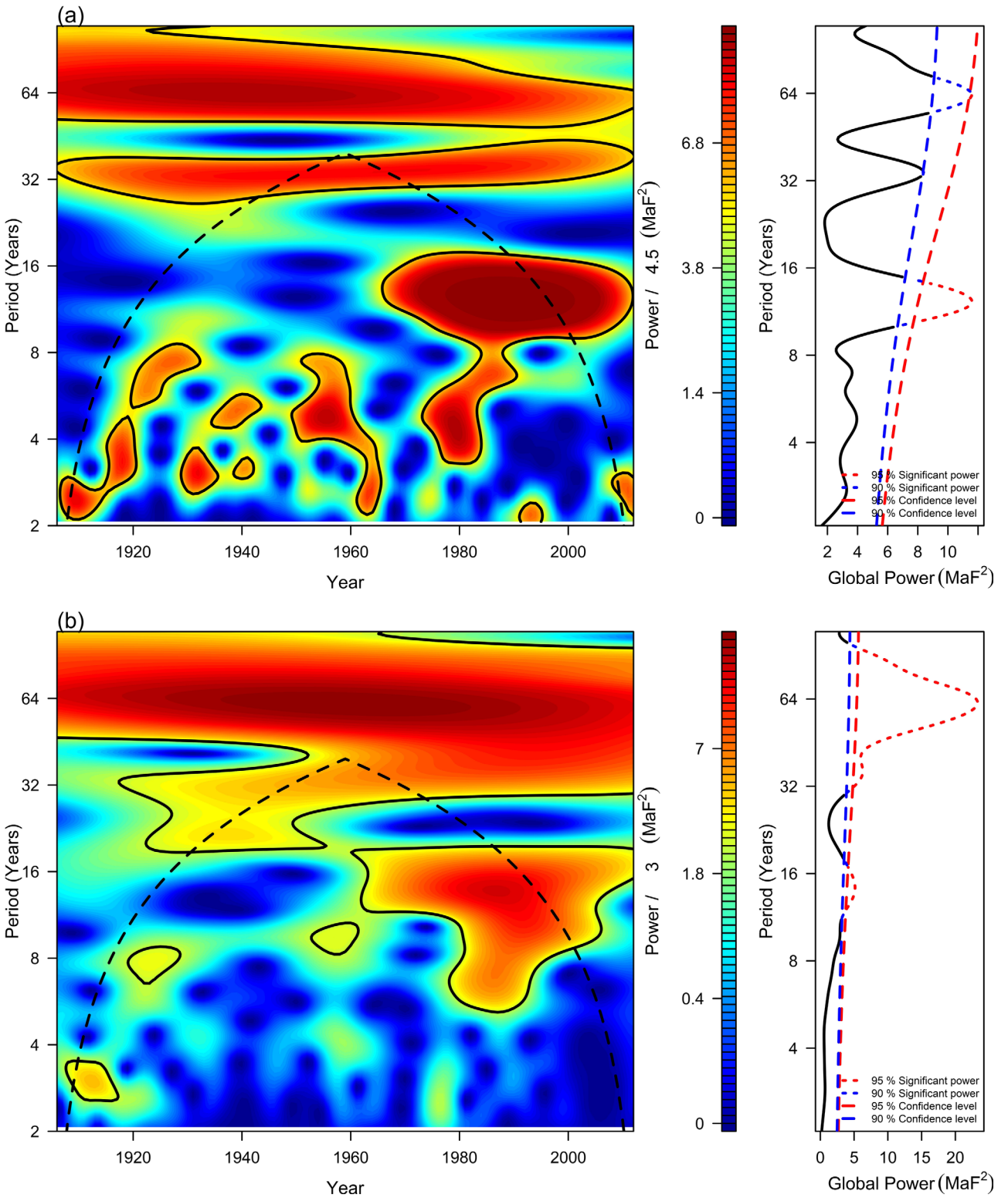

Figure 10. Power spectra of the Lees Ferry flow (a) from the median of the simulations (b) historical (1906–2012) flow—local spectrum on the left and global on the right.

The spectra of the median flows from the simulations and the historical flows are shown in Figure 10. The nonstationarity in the spectrum—especially the power in the 8–16 year period in recent decades is very well captured by the simulations. The global spectrum (figures on the right in both the plots), also, is simulated well, although the amplitude of the median peaks is smaller. The fact that the nonstationarity in the

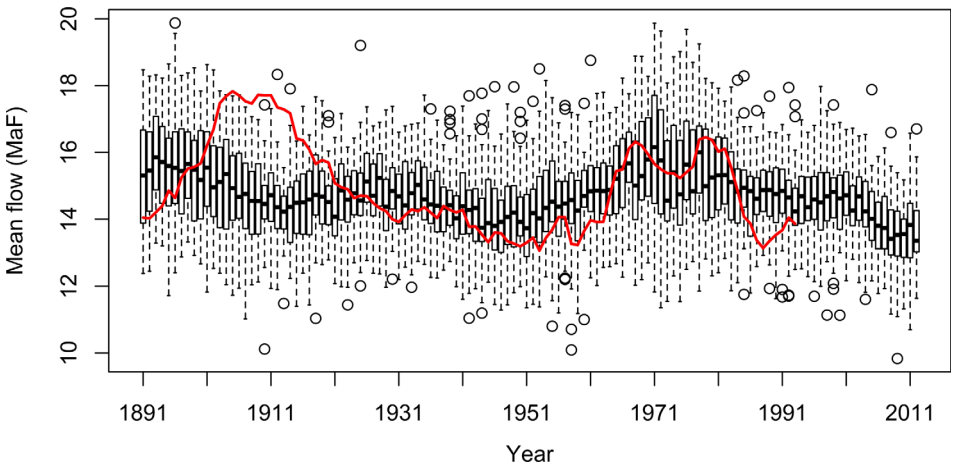

Figure 11. Time series plots of the Projections. The box plots are the 20 year mean projections and red line is the 20 year mean historical flow at Lees Ferry. The 20 year mean historical flow (red) stops in 1991 (which corresponds to 1991–2010 mean flow) and the 20 year mean projections continue until 2010.

flow spectrum is captured purely from the climate indices is remarkable. We point out that the simulation methodology is not designed to reproduce the spectrum or distributional properties of the flows as the flows are simulated as a consequence from the climate indicators. The median of all the spectra for each time and period was found to be similar to the spectrum of the median flows from the simulations described in Figure 10.

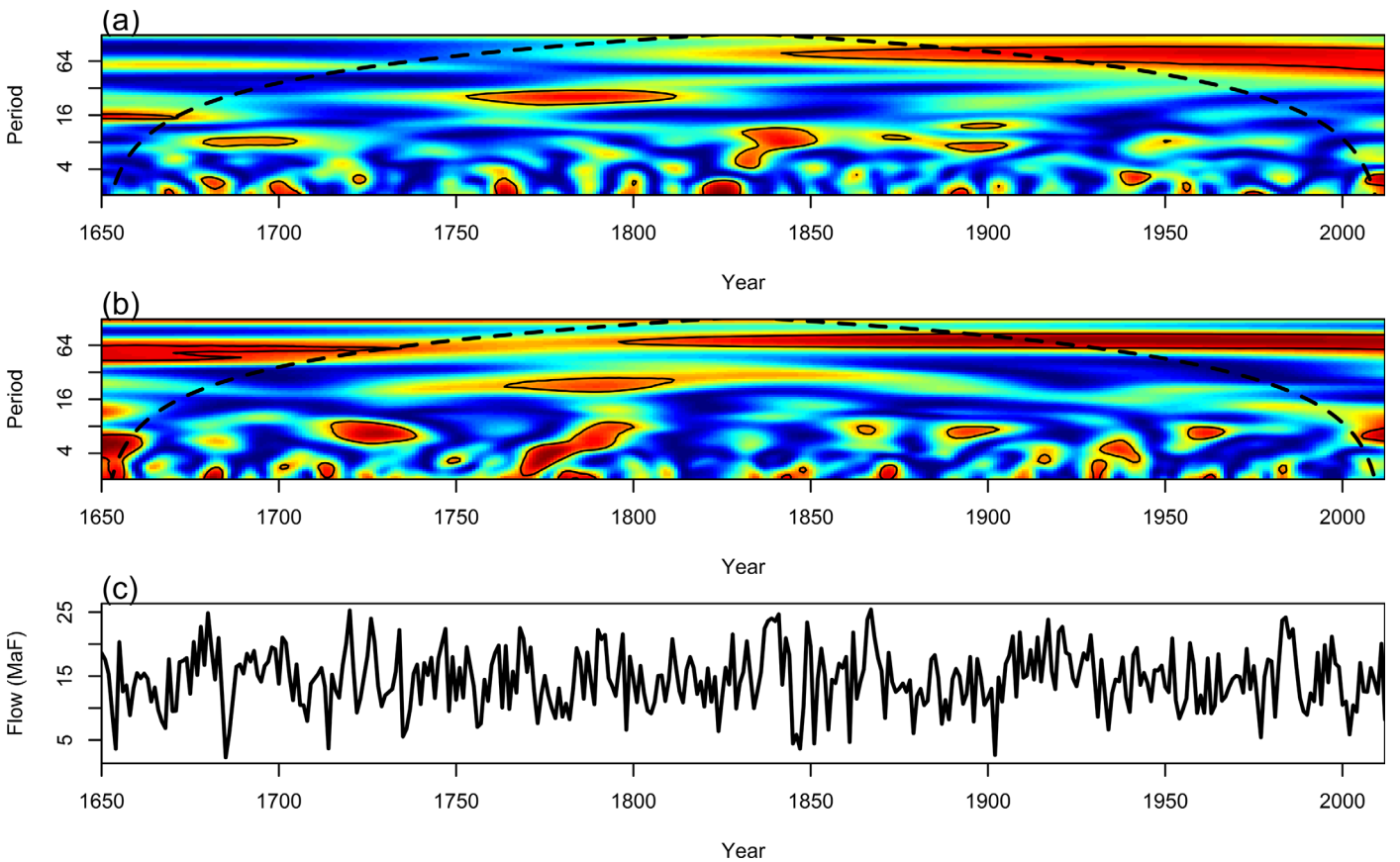

Figure 12. (a) Coherence plots of long historical (1650–2012) Lees Ferry flow with AMO; (b) is same as Figure 12a but the coherence of the Lees Ferry flow with PDO; (c) time series plot of long historical Lees Ferry flow.

The decadal (8–16 year period) variability, is not significant in the global spectra of the climate indices (Figure 1a and Figure 2a), but in recent decades it is significant in the spectrum of PDO (Figure 2a). However, the coherence of Lees Ferry flow with AMO and PDO clearly show the multi-decadal (32–100 year) association with AMO and PDO (Figure 12a and 12b) and association at the 8–16 year period in recent decades with PDO (Figure 12b). This significant coherence of Lees Ferry flow with PDO in the 8–16 year period as seen in Figure 12b in recent years suggests the modulating effect of PDO on the Colorado River flow at decadal time scales.

5.3. Lees Ferry Streamflow Conditional Projections

The proposed simulation model described and validated in previous sections also has the potential for applications to short-term ensemble projections. This section is intended to demonstrate this potential and for detailed skill analysis and comparison with other methods we refer the readers to *Erkyihun* [2015]. We generated ensembles of 20 year projections for each year starting from 1890 using the methodology as described above. The ensembles of projected 20 year mean flows are shown as boxplots and the 20 year mean flow from history is shown as solid line (Figure 11). It can be seen that the ensembles reproduce the observed temporal characteristic of the 20 year mean flows very well. However, the high flows during the early part of the record (1906–1920) are under simulated. This is due to the fact that the flow simulation is based on bootstrapping past flows and, for this period, the flows are large relative to pre-1906 flows which do not include a sustained period of very high flows. Another reason is that the high flow periods in the past should coincide with the climate forcings, else the neighbors selected based on climate variables will not correspond well with high flows for resampling. The sustained wet period of 1906–1920 has good coherence with the AMO and PDO anomalies in the 64 year period band (Figure 12). The 20 year projections of climate indices for the 1906–1920 epoch are resampled mostly from ~1840 (64 years back from 1906) which is the nearest neighbor to the climate indices at the start of 1906. Thus, the flows are also simulated largely from this period, which is relatively lower. The projections perform very well from 1920 to 1960, where we do not have extreme wet periods sustained periods. The 1980s wet period is captured by the projections as well. This wet period is not sustained for longer period as in the early 1900s and resampling was possible from the past paleodata as well as from the early 1900s wet period.

5.4. Limitation of the WKNN

The WKNN method relies on the strength of the teleconnections between large-scale climate forcings and streamflow, as the streamflow is resampled conditioned on the climate forcing. The assumption is made that the climate forcings are independent, which they are in this case, thus justifying simulating them independently. If the forcings are correlated, then they have to be simulated jointly, which requires modification of the methodology. If the length of the time series is short, then lower frequency signals cannot be simulated with enough variety. For short-term projections, the flow is resampled from the past based on the neighbors of the projected climate forcings. Thus, if the past does not include sustained wet or dry periods corresponding to the projected climate forcings, then the flow projections will be lower or higher, respectively. This was seen in the 1906–1920 projections above.

6. Summary and Discussion

As the anthropogenic climate change discussion has become mainstream, the climate sensitivity of hydrologic time series has evinced considerable interest. By and large, the dynamic range of hydroclimatic variation over the last millennium in places such as Colorado River Basin appears to be much larger than the relatively modest, yet uncertain, projections from a chain of coupled models of the ocean-atmosphere and hydrology [*Switanek and Troch*, 2011]. Specifically, the physics-based models do not adequately reproduce the interannual, decadal, and multidecadal variations that are in evidence from tree rings, and the associated reconstructions of hydrology of the region. As a result, water managers seek methods by which storage needed to meet demand and, correspondingly, the potential reliability and resilience of existing projects relative to these climate variations, can be assessed. This is the context for the methods developed and exemplified in this paper.

The causal framework for low frequency variations in regional streamflow suggests that these variations are derived from like variations in large-scale climate phenomena such as the AMO and the PDO. Consequently,

the need to develop long-term, stochastic simulations of those indices emerged as a first step in developing an approach for low-frequency simulations of the streamflow, and led to the strategy presented here. The WKNN method developed was applied in this manner and also directly to the 107 years of Colorado River naturalized flows at Lees Ferry (figures not shown). The direct application led to performance considerably poorer than the application following the climate causal framework, suggesting that using the paleoproxies for the climate indices and then conditioning the streamflow on the simulated indices is superior to a direct attempt to model low-frequency variability in the streamflow series. This is very interesting since the AMO, PDO, ENSO, and North Atlantic Oscillation (NAO) have seen significant efforts at paleoreconstruction and collectively influence hydrology over much of North America and parts of Europe and Asia. Developing a library of the simulations of these indices may then allow local investigators the ability to use the appropriate indices to conditionally simulate streamflow with the proper low frequency character. This model can be combined with simulations of climate forcings from global climate models to exploit the teleconnections at longer-time scales. In future work, we plan to explore the application to other settings, and to extend our prior work on multivariate simulation [*Lall et al*., 2015] to this setting as well.

Acknowledgments
The authors thankfully acknowledge the funding for this research by the Bureau of Reclamation (R12AC30023). We are grateful for inputs and support from James Prairie. Insights and comments from three anonymous reviewers significantly improved the manuscript, for which we are very thankful. To obtain the data used to produce the results of this paper, please follow the links and descriptions in the data section.

References

Bracken, C., B. Rajagopalan, and E. Zagona (2014), A Hidden Markov model combined with climate indices for multi-decadal streamflow simulation, *Water Resour. Res.*, *50*, 7836–7846, doi:10.1002/2014WR015567.

Caraway, N. M., J. L. McCreight, and B. Rajagopalan (2014), Multisite stochastic weather generation using cluster analysis and k-nearest neighbor time series resampling, *J. Hydrol. 508*, 197–213, doi:10.1016/j.jhydrol.2013.10.054.

Dracup, J. A., and E. Kahya (1994), The relationships between United States streamflow and La Niña events, *Water Resour. Res.*, *30*, 2133–2141, doi:10.1029/94WR00751.

Efron, B., and R. Tibishirani (1993), *An Introduction to the Bootstrap*, Chapman and Hall, N. Y.

Enfield, D. B., A. M. Mestas-Nunez, and P. J. Trimble (2001), The Atlantic multidecadal oscillation and its relation to rainfall and river flows in the continental US, *Geophys. Res. Lett.*, *28*, 2077–2080, doi:10.1029/2000GL012745.

Erkyihun, S. T. (2015), Multi-Decadal stochastic streamflow projection an application to water resources decision making in the Colorado River Basin, Civil, Environmental, and Architectural Engineering, PhD. thesis, Univ. of Color., Boulder.

Gangopadhyay, S., B. L. Harding, B. Rajagopalan, J Lukas, and T Fulp (2009), A nonparametric approach for paleohydrologic reconstruction of annual streamflow ensembles, *Water Resour. Res.*, *45*, W06417, doi:10.1029/2008WR007201.

Gershunov, A., and T. P. Barnett (1998), Interdecadal modulation of ENSO teleconnections, *Bull. Am. Meteorol. Soc.*, *79*, 2715–2725, doi:10.1175/1520-0477(1998)079<2715:IMOET>2.0.CO;2.

Grantz, K., B. Rajagopalan, M. Clark, and E. Zagona (2005), A technique for incorporating large-scale climate information in basin-scale ensemble streamflow forecasts, *Water Resour. Res.*, *41*, W10410, doi:10.1029/2004WR003467.

Gray S. T., L. J. Graumlich, J. L. Betancourt, and G. T. Pederson (2004), A tree-ring based reconstruction of the Atlantic Multidecadal Oscillation since 1567 A.D., *Geophys. Res. Lett.*, *31*, L12205, doi:10.1029/2004GL019932.

Hidalgo, H. G. (2004), Climate precursors of multidecadal drought variability in the western United States, *Water Resour. Res.*, *40*, W12504, doi:10.1029/2004WR003350.

Kaplan, A., M. A. Cane, Y. Kushnir, A. C. Clement, M. B. Blumenthal, and B. Rajagopalan (1998), Analyses of global sea surface temperature 1856–1991, *J. Geophys. Res.*, *103*, 18,567–18,589, doi:10.1029/97JC01736.

Kumar, P., and E. Foufoula-Georgiou (1997), Wavelet analysis for geophysical applications, *Rev. Geophys.*, *35*, 385–412, doi:10.1029/97RG00427.

Kumar, P., and E. Foufoula-Georgiou (1994), Introduction to wavelet transforms, in *Wavelets in Geophysics*, edited by E. Foufoula-Georgiou and P. Kumar, Academic press, Inc., San Diego, Calif.

Kwon, H. H., U. Lall, and A. F. Khalil (2007), Stochastic simulation model for nonstationary time series using an autoregressive wavelet decomposition: Applications to rainfall and temperature, *Water Resour. Res.*, *43*, W05407, doi:10.1029/2006WR005258.

Lall, U. (1995), Recent advances in nonparametric function estimation: Hydrologic applications, *Rev. Geophys.*, *33*, 1093–1102, doi:10.1029/95RG00343.

Lall, U., and, A. Sharma (1996), A nearest Neighbor bootstrap for resampling hydrologic time series, *Water Resour. Res.*, *32*, 679–693, doi:10.1029/95WR02966.

Lall, U., N. Devineni, and Y. Kaheil (2015), An empirical, nonparametric simulator for multivariate random variables with differing marginal densities and nonlinear dependence with hydroclimatic applications, *Risk Anal.*, *36*, 57–73, doi:10.1111/risa.12432.

Loucks, D. P., and E. Van Beek (2005), Concepts in Probability, statistics and stochastic modelling, in *Water Resources Systems Planning and Management*, pp. 169–229, UNESCO Publ., U. N. Educ., Sci. and Cult. Organ., Delft, Netherlands.

MacDonald, G. M., and R. A. Case (2005), Variations in the Pacific decadal oscillation over the past millennium, *Geophys. Res. Lett.*, *32*, L08703, doi:10.1029/2005GL022478.

Mantua, N. J., S. R. Hare, Y. Zhang, J. M. Wallace, and R. C. Francis (1997), A Pacific interdecadal climate oscillation with impacts on salmon production. *Bull. Am. Meteorol. Soc.*, *78*, 1069–1079, doi:10.1175/1520-0477(1997)078<1069:APICOW>2.0.CO;2.

McCabe, G. J., and M. D. Dettinger (1999), Decadal variations in the strength of ENSO teleconnections with precipitation in the western United States, *Int. J. Climatol.*, *19*, 1399–1410, doi:10.1002/(SICI)1097-0088(19991115)19:13<1399::AID-JOC457>3.0.CO;2-A.

McCabe, G. J., M. A. Palecki, and J. L. Betancourt (2004), Pacific and Atlantic Ocean influences on multidecadal drought frequency in the United States, *Proc. Natl. Acad. Sci. U. S. A.*, *101*(12), 4136–4141.

McCabe, G. J., J. L. Betancourt, and H. G. Hidalgo (2007), Associations of decadal to multidecadal sea surface temperature variability with Upper Colorado River flow, *J. Am. Water Resour. Assoc.*, *43*, 183–192, doi:10.1111/j.1752-1688.2007.00015.x.

McCabe, G. J., S. T. Gray, M. A. Palecki, and H. G. Hidalgo (2008), Associations of multi-decadal sea surface temperature variability with US drought, *Quat. Int.*, *188*, 31–40, doi:10.1016/j.quaint.2007.07.001.

Miller, W., R. Butler, T. Piechota, J. Prairie, K. Grantz, and G. DeRosa (2012), water management decisions using multiple hydrologic models within the San Juan River Basin under Changing climate conditions, *J. Water Resour. Plann. Manage.*, *138*, 412–420, doi:10.1061/(ASCE)WR.1943-5452.0000237.

Nowak, K., B. Rajagopalan, and E. Zagona (2011), Wavelet Auto-Regressive Method (WARM) for multi-site streamflow simulation of data with non-stationary spectra, *J. Hydrol.*, *410*(1–2), 1-12, doi:10.1016/j.jhydrol.2011.08.051.

Nowak, K., M. Hoerling, B. Rajagopalan, and E. Zagona (2012), Colorado River basin hydroclimatic variability, *J. Clim.*, *25*, 4389–4403, doi:10.1175/JCLI-D-11-00406.1.

Prairie, J., and R. Callejo (2005), *Natural Flow and Salt Computation Methods*, U.S. Bur. the Inter., Salt Lake City, Utah.

Politis, D. N., and J. P. Romano (1994), The stationary bootstrap, *J. Am. Stat. Assoc.*, *89*(428), 1303–1313, doi:10.1080/01621459.1994.10476870.

Rajagopalan, B., and U. Lall (1999), A k-nearest-neighbor simulator for daily precipitation and other weather variables, *Water Resour. Res.*, *35*, 3089–3101, doi:10.1029/1999WR900028.

Rajagopalan, B., E. Cook, U. Lall, and B. K. Ray (2000), Spatiotemporal variability of ENSO and SST teleconnections to summer drought over the United States during the twentieth century, *J. Clim.*, *13*, 4244–4255, doi:10.1175/1520-0442(2000)013<4244:SVOEAS>2.0.CO;2.

Razavi, S., A. Elshorbagy, H. Wheater, and D. Sauchyn (2015), Toward understanding nonstationarity in climate and hydrology through tree ring proxy records, *Water Resour. Res.*, *51*, 1813–1830, doi:10.1002/2014WR015696.

Reclamation (2012), *Colorado River Basin Water Supply and Demand Study*, U.S. Dep. of the Inter. Bur. of Reclam, Washington, D. C.

Redmond, K. T., and R. W. Koch (1991), Surface climate and streamflow variability in the western United States and their relationship to large-scale circulation indices, *Water Resour. Res.*, *27*, 2381–2399, doi:10.1029/91WR00690.

Regonda, S., E. Zagona, and B. Rajagopalan (2011), Prototype decision support system for operations on the Gunnison basin with improved forecasts, *J. Water Resour. Plann. Manage.*, *137*, 428–438, doi:10.1061/(ASCE)WR.1943-5452.0000133.

Regonda, S. K., B. Rajagopalan, M. Clark, and E. Zagona (2006), A multimodel ensemble forecast framework: Application to spring seasonal flows in the Gunnison River Basin, *Water Resour. Res.*, *42*, W09404, doi:10.1029/2005WR004653.

Salas, J. D., J. W. Delleur, V. Yevjevich, and W. L. Lane (1980), *Applied Modeling of Hydrological Time Series*, Water Resour. Publ., Littleton, Colo., 484 pp.

Sharma, A., D. G. Tarboton, and U. Lall (1997), Streamflow simulation: A nonparametric approach, *Water Resour. Res.*, *33*, 291–308, doi:10.1029/96WR02839.

Steinman B. A, M. E. Mann, and S. K. Miller (2015), Atlantic and Pacific multidecadal oscillations and North Hemisphere temperatures, *Science*, *347*(6225), 988–991, doi:10.1126/science.1257856.

Switanek, M. B., and P. A. Troch (2011), Decadal prediction of Colorado River streamflow anomalies using ocean–atmosphere teleconnections, *Geophys. Res. Lett.*, *38*, L23404, doi:10.1029/2011GL049644.

Thomas, B. E. (2007), Climatic fluctuations and forecasting of streamflow in the Lower Colorado River basin. *J. Am. Water Resour. Assoc.*, *43*, 1550–1569, doi:10.1111/j.1752-1688.2007.00127.x.

Thomson, A. M., R. A. Brown, N. J. Rosenberg, R. C. Izaurralde, D. M. Legler, and R. Srinivasan (2003), Simulated impacts of El Nino southern oscillation On United States water resources. *J. Am. Water Resour. Assoc.*, *39*, 137–148, doi:10.1111/j.1752-1688.2003.tb01567.x.

Timilsena, J., T. Piechota, G. Tootle, and A. Singh (2009), Associations of interdecadal/interannual climate variability and long-term Colorado River basin streamflow, *J. Hydrol.*, *365*, 289–301, doi:10.1016/j.jhydrol.2008.11.035.

Tootle, G. A., T. C. Piechota, and A. Singh (2005), Coupled oceanic–atmospheric variability and U.S. streamflow, *Water Resour. Res.*, *41*, W12408, doi:10.1029/2005WR004381.

Torrence, C., and G. P. Compo (1998), A practical guide to wavelet analysis, *Bull. Am. Meteorol. Soc.*, *79*, 61–78, doi:10.1175/1520-0477(1998)079<0061:APGTWA>2.0.CO;2.

Towler, E., B. Rajagopalan, C. Seidel, and R. S. Summers (2009), Simulating ensembles of source water quality using a k-nearest neighbor resampling approach, *Environ. Sci. Technol.*, *43*, 1407–1411, doi:10.1021/es8021182.

Vogel, R. M., and A. L. Shallcross (1996), The moving blocks bootstrap versus parametric time series models, *Water Resour. Res.*, *32*, 1875–1882, doi:10.1029/96WR00928.

Wei, W. W. S. (2006), *Time Series Analysis - Univariate and Multivariate Methods*, Pearson Addison-Wesley, Boston, 614 pp.

Woodhouse C. A., S. T. Gray, and D. M. Meko (2006), Updated streamflow reconstructions for the Upper Colorado River Basin, *Water Resour. Res.*, *42*, W05415, doi:10.1029/2005WR004455.

Yates, D., S. Gangopadhyay, B. Rajagopalan, and K. Strzepek (2003), A technique for generating regional climate scenarios using a nearest-neighbor algorithm, *Water Resour. Res.*, *39*(7), 1199, doi:10.1029/2002WR001769.

Zhang, Y., J. M. Wallace, and D. S. Battisti (1997), ENSO-like interdecadal variability: 1900-93, *J. Clim.*, *10*, 1004–1020, doi:10.1175/1520-0442(1997)010 < 1004:ELIV>2.0.CO;2.